




Surface Diffusion and the Interfacial Reaction in Cu/Sn/Ni Micro-Pillars

H.Y. YU,¹ T.H. YANG,¹ Y.S. CHIU,¹ and C.R. KAO ^{1,2,3}

1.—Department of Materials Science and Engineering, National Taiwan University Taipei, Taipei, Taiwan. 2.—Advanced Research Center for Green Materials Science and Technology, National Taiwan University Taipei, Taipei, Taiwan. 3.—e-mail: crkao@ntu.edu.tw

An electroplated Cu/Sn/Ni micro-bump was fabricated for analysis. After aging for different times, both the morphology and microstructure show significant changes, particularly after long-term aging. Because of the small aspect ratio of the micro-bump, surface diffusion has a strong effect on the morphology and roughness of the Cu/Sn and Cu/IMCs interfaces. A focused ion beam was applied for 3D reconstruction and used for calculation of the voiding rate of the micro-joint after 720 h of aging. In this way, the relationship between the voiding rate redistribution and the position along the radius direction was obtained. It is concluded that the redistribution of voids after long time aging is controlled by surface diffusion when almost all of the intermetallic compounds (IMCs) in the Cu/Sn/Ni micro-bump were transformed to Cu₃Sn. Furthermore, as observed from the relationship between the voiding rate of the 5 μm and 10 μm samples and the position along the radius, when the diameter of the micro-bump decreases to 5 μm or even less than 5 μm, the total voiding rate of the sample after long-term aging rapidly increases, and a higher voiding rate has a strong influence on the reliability of the micro-joint and may lead to the failure of the electronic device.

Key words: (Cu,Ni)₆Sn₅, surface diffusion, 3D reconstruction, voiding rate, reliability

INTRODUCTION

It is well-known that Pb has a serious impact on environment and human health, which led to the prohibition of the use of lead-based solder in the electronics industry in 2003. Because of their good quality and low cost, Sn/Cu solders are becoming a great alternative for use in electronic packaging and have been studied extensively during the last several decades. Tu^{1,2} studied the kinetics of the Cu/Sn interfacial reaction, and reported the different kinetics models of Cu₆Sn₅ and Cu₃Sn phase formation in solid-state aging. According to the results reported by Kao,³ for solid-liquid reactions, the growth of Cu/Sn intermetallic compounds

(IMCs) is controlled by diffusion. Furthermore, using transmission electron microscopy (TEM), Chung and Kao⁴ provided direct evidence for a Cu-enriched region at the boundary between Cu₆Sn₅ and Cu₃Sn and described, in detail the formation of η-Cu₆Sn₅. With the development of the 3C industry, the wide application of electroplated copper has led to the observation of the appearance of Kirkendall voids near the interface. Zeng⁵ found that a large number of Kirkendall voids formed in the Cu₃Sn layer and that these voids can weaken the solder joint. Yu⁶ proposed that residual S segregation to the Cu/Cu₃Sn interface accelerates the formation of Kirkendall voids, and Wang⁷ found that impurities in the electroplated Cu maybe the main factor that gives rise to the formation of Kirkendall voids. In 2010, Yin⁸ verified Wang's hypothesis experimentally and showed that the impurities in electroplated copper are the origin of the Kirkendall effect.

(Received April 11, 2019; accepted July 17, 2019;
published online July 29, 2019)

The diffusion and nucleation of impurities leads to the Kirkendall effect. Therefore, diffusion in the Cu/Sn system plays an important role in the reliability issues.

In the twenty-first century, the increasing demand for high-performance of electronic devices has become the strongest driving force in the electronic industry. However, due to Moore's Law reaching its limit, during the past 10 years, through-silicon via (TSV) and micro-bump of three-dimensional integrated circuit (3D-IC) integration technology has become a possible approach to go beyond Moore's Law. Additionally, Ni acting as a diffusion barrier has become an important part of micro-joints. Because of its good stability and lower cost, the use of the Cu/Sn/Ni micro-bump is currently the most popular approach in 3D-IC integration technology. Numerous researchers have reported their studies about the Cu/solder/Ni structure since 2004. Ho and Kao⁹⁻¹¹ found in the Cu/solder/Ni system that $(\text{Cu,Ni})_6\text{Sn}_5$ formed on both the Ni side and the Cu side and illustrated the reason for the $(\text{Cu,Ni})_6\text{Sn}_5$ formation. In 2008, Nogita¹² showed that in a Cu/Sn/Ni system, Ni can stabilize hexagonal $(\text{Cu,Ni})_6\text{Sn}_5$, and over the next few years, Nogita's group carried out many studies of do many researches about η - $(\text{Cu,Ni})_6\text{Sn}_5$ and η' - $(\text{Cu,Ni})_6\text{Sn}_5$ ¹³⁻¹⁵ involving the kinetics of the η - η' transformation and comparisons of the thermal expansion and mechanical properties of Cu_6Sn_5 and $(\text{Cu,Ni})_6\text{Sn}_5$. However, almost all of the studies on $(\text{Cu,Ni})_6\text{Sn}_5$ and Cu/Sn/Ni systems have focused on the bump size of ball grid array (BGA) and flip chips, and only a few studies have examined the micro-joint. Recently, Mo¹⁶ found that under certain reflow conditions, an ultra-high Ni content $(\text{Cu,Ni})_6\text{Sn}_5$ phase is found in the middle of the sample in the micro-bump even after all of the joint has been transformed to Cu_3Sn . This result motivates us to investigate several open questions, such as phase formation and diffusion behavior, which must be examined for the Cu/Sn/Ni system, particularly in micro-joints. It is well-known that due to the small aspect ratio of the micro-bump, surface diffusion cannot be ignored.^{17,18} However, there has been no report to date on the diffusion behaviors near the free surface, and it is unclear whether there is any change in the material after all of the solder in the micro-bump has become Cu_3Sn .

In our previous research, Yang^{19,20} reported that for both Ni/Sn/Ni solid-state aging and the Cu/Sn/Ni solid-liquid reaction, the surface diffusion phenomenon is clearly observed. However, for solid-liquid reactions, dissolution and sidewall wetting can have strong impacts on the microstructure and morphology near the free surface. Therefore, the objectives of the present study are to confirm the influence of surface diffusion on the Cu/Sn/Ni structure and to observe and analyze whether any special phenomena are present after long-term solid-state aging.

EXPERIMENTAL PROCEDURE

In this study, Cu/Sn/Ni micro-bumps were fabricated by electroplating on a 4 inch Si wafer with pre-sputtered Cr/Cu seed layers, as shown in Fig. 1. The diameter of each pillar was $30\ \mu\text{m}$, and the thickness of each layer is also shown in figure. The wafer was diced into $8\ \text{mm} \times 8\ \text{mm}$ dies, with 400 micro-bumps obtained from each die. Figure 2a shows the top view of the die with micro-bumps, and Fig. 2b shows an enlarged view of the micro-bumps. Then, after polishing, the cross-section image of the micro-bump is shown in Fig. 2c. After dicing, the samples were aged in a furnace at 180°C for 2, 8, 24, 72, 144, 288, 360, and 480 h, and the longest aging time reached 1000 h. Scanning electron microscopy (JeoL JSM-7800F Prime) was used to characterize the morphological and microstructural changes after a solid-state reaction. In addition, to verify the effect of surface diffusion, scanning Auger spectroscopy was used to identify the distributions of copper and tin. To determine whether there were any voids in the micro-pillar after long-term aging, focus ion beam was used to reconstruct 3D structure of the micro-bump. Furthermore, electron probe microscopy analysis (EPMA) was used to analyze the element distribution and phase composition.

RESULTS AND DISCUSSION

Figure 3a, b, c, and d shows the side views of the samples after aging for 2, 24, 72, and 360 h, respectively. As can be observed from Fig. 2b, after electroplating the Cu/Sn/Ni sandwich structure is a planar structure. However, after aging for 2 h, Cu_6Sn_5 appears to grow along the Cu/Sn interface, and the interface becomes rough. Figure 3b, c, and d shows that as the aging time continued to increase, the growth of Cu_6Sn_5 near the Cu/Sn and Cu/IMC interface become increasingly more significant. As mentioned in previous reports,^{17,18} when the aspect ratio of the micro-bump becomes sufficiently small, surface diffusion becomes important and affects the morphology of the sample, particularly for the solid-state reaction. Additionally, it is known that Cu is the dominant diffusing species in the Cu/Sn/Ni solid-state reaction.¹ Therefore, it is assumed that Cu diffuses to the Sn layer to form Cu_6Sn_5 and it is easier for the Cu atom near the free surface to react with Sn at the edge of the pillar, which leads to the stronger consumption of Cu near the surface as compared to that of Cu in the middle of the micro-bump. Finally, after this process, Cu_6Sn_5 near the Cu/Sn interface can be clearly observed and the Cu/Sn interface becomes rough. Figure 3e, f, g, and h shows the cross-section BSE images of the samples corresponding to Fig. 3a, b, c, and d, respectively. This assumption is verified based on the consumption of Cu observed in Fig. 3e, f, and g. Furthermore, Fig. 3e, f, and g shows that some Sn residue after aging for 2 h and a thin layer of Cu_6Sn_5 could

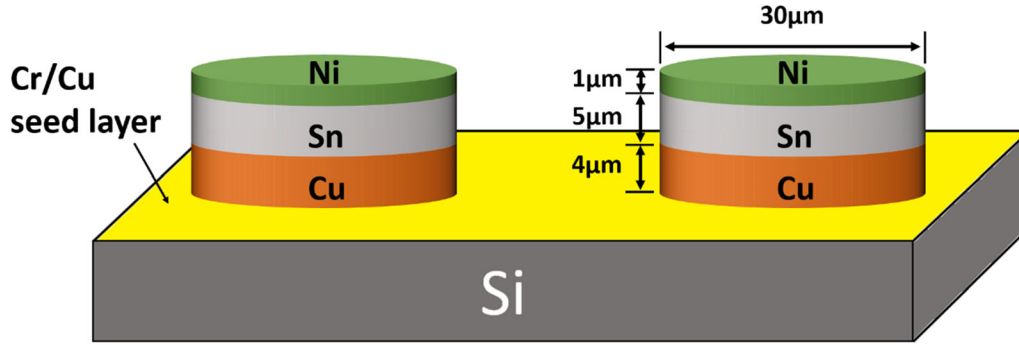


Fig. 1. Schematic illustration showing the Cu/Sn/Ni structure in this study.

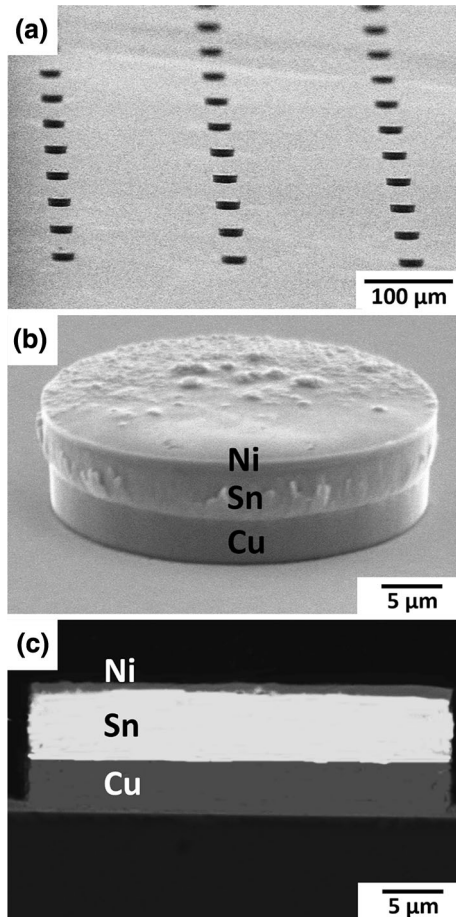


Fig. 2. Real sample after electroplating (a) overall; (b, c) sample before and after polishing, respectively.

to be found in both Ni/Sn side and Cu/Sn side. When the aging time reached 24 h, all of the Sn was converted to Cu_6Sn_5 , and a thin Cu_3Sn layer was observed with some Kirkendall voids. After aging for 72 h, the Cu_3Sn layer becomes thicker. In Fig. 3h, after 360 h of aging, Cu_3Sn becomes the dominant phase in the micro-bump with some Cu_6Sn_5 phase (bright contrast) found both at the middle of the micro-bump and near the Ni side. Moreover, the bright contrast can still be observed at the middle of the micro-bump after aging for

1000 h. SEM EDS was used to perform a preliminary identification of the phase, and the brighter phase is identified as $(\text{Cu},\text{Ni})_6\text{Sn}_5$. The morphology of the sample shows significant changes, after the aging process with many voids formed near the free surface.

To determine the exact composition of $(\text{Cu},\text{Ni})_6\text{Sn}_5$, EPMA was used. In Fig. 4, it can be clearly observed that, after aging for 144 h, some $(\text{Cu},\text{Ni})_6\text{Sn}_5$ is surrounded by Cu_3Sn , and that Cu_3Sn grew along the Cu_6Sn_5 's grain boundary. Finally, EPMA WDS was used to analyze points A, B and C in Fig. 4. Table I presents the EPMA results of the compositions of the IMCs at the positions A, B and C. As seen from the table, even though it is confirmed that the points at A and C are identified as $(\text{Cu},\text{Ni})_6\text{Sn}_5$, both $(\text{Cu},\text{Ni})_6\text{Sn}_5$ phase contain very different Ni contents. The $(\text{Cu},\text{Ni})_6\text{Sn}_5$ located at point C, which is surrounded by Cu_3Sn , contains much higher Ni contents than the $(\text{Cu},\text{Ni})_6\text{Sn}_5$ located at point A, near the Ni side. From the isothermal section at 125°C of the Cu/Sn/Ni ternary phase diagram obtained by a Japanese research team,²¹ it can be concluded that when the solubility of Ni content reaches its maximum, $(\text{Cu},\text{Ni})_6\text{Sn}_5$ will not change to Cu_3Sn , and that the maximum solubility of Ni content in Cu_3Sn is much lower than in Cu_6Sn_5 . The presence of $(\text{Cu},\text{Ni})_6\text{Sn}_5$ at the middle and near the Ni side of the micro-bump can be explained based on the Cu/Sn/Ni ternary phase diagram. When Cu_6Sn_5 changes to Cu_3Sn , due to the difference in the maximum solubility limit of Ni content, the excess Ni atoms were diffused along the Cu_6Sn_5 grain boundary, thereby increasing the Ni content in $(\text{Cu},\text{Ni})_6\text{Sn}_5$ at the middle of the micro-bump. After the Ni content of $(\text{Cu},\text{Ni})_6\text{Sn}_5$ reaches its maximum solubility, $(\text{Cu},\text{Ni})_6\text{Sn}_5$ becomes a stable phase and the Cu atoms from the Cu side cannot react with it, so these Cu atoms must go around this high-Ni-content $(\text{Cu},\text{Ni})_6\text{Sn}_5$ and diffuse to other side to form Cu_3Sn . Consequently, the high-Ni-content $(\text{Cu},\text{Ni})_6\text{Sn}_5$ is formed at the middle of the micro-bump and surrounded by Cu_3Sn . In addition, a stable $(\text{Cu},\text{Ni})_6\text{Sn}_5$ with high Ni content also formed near the Ni side due to the abundant supply of Ni.

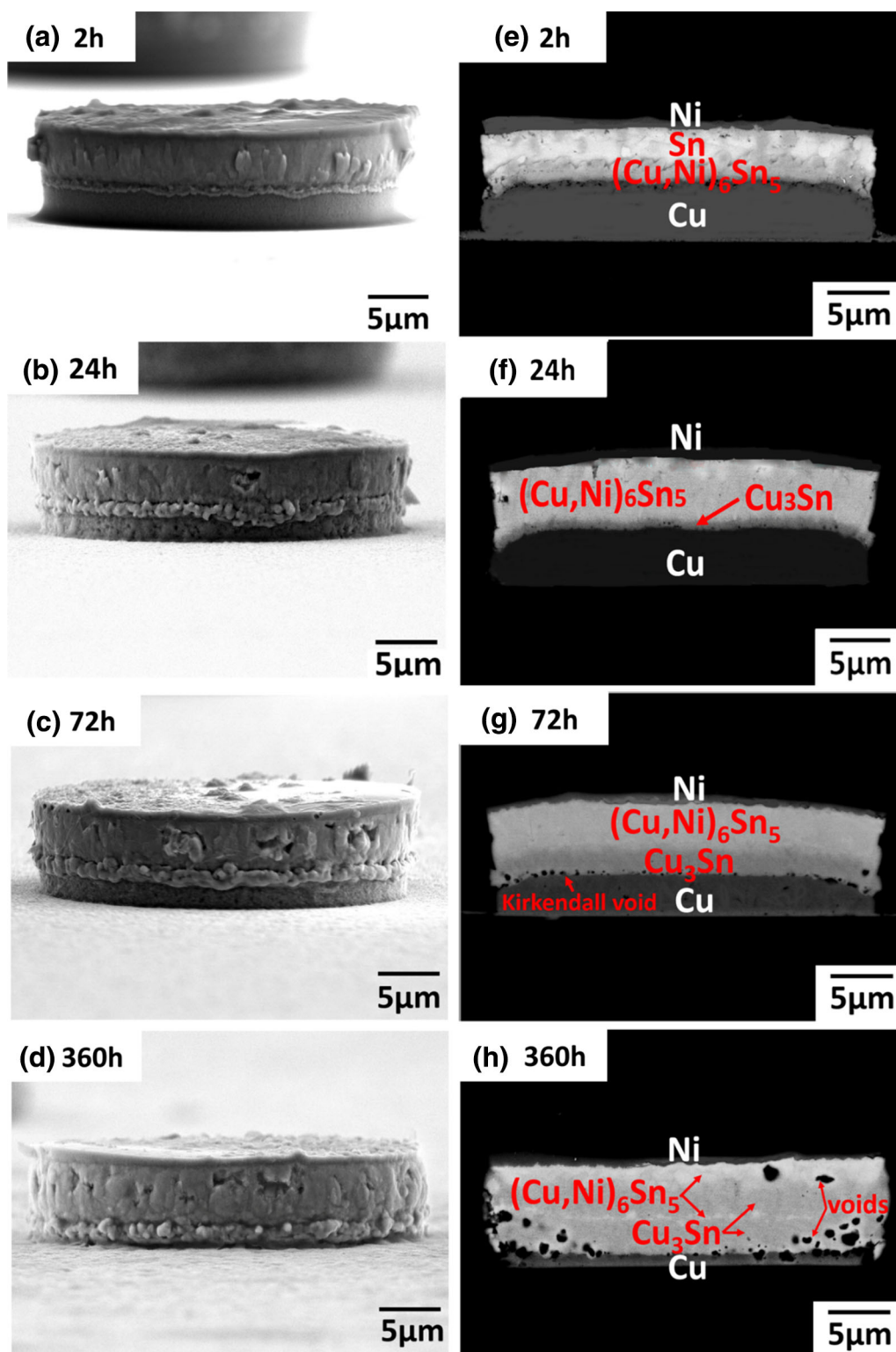


Fig. 3. Side views of the sample after aging in air at 180°C for (a) 2 h, (b) 24 h, (c) 72 h, (d) 360 h; cross-section BSE images of the same sample after (e) 2 h, (f) 24 h, (g) 72 h, (h) 360 h.

In Mo's study,¹⁶ a high-Ni-content $(\text{Cu,Ni})_6\text{Sn}_5$ was also observed under certain solid-liquid reaction conditions. Further experiments must be performed to analyze and observe the microstructure of this phase.

Scanning Auger spectroscopy was used to analyze the effect of surface diffusion, and the sample that was aged for 72 h was chosen for analysis because the interface was rough and surface diffusion can be easily seen. Figure 5a shows the sample for Ar-ion

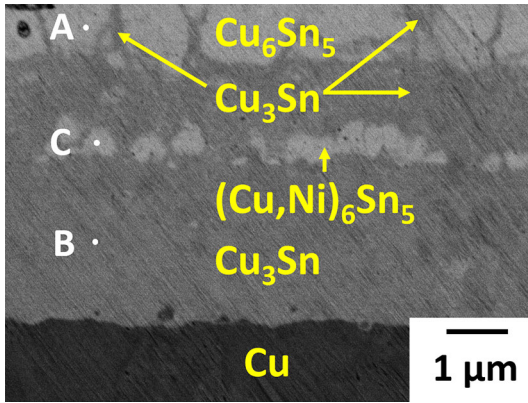


Fig. 4. Cross-section BSE image of the sample after 144 h of aging.

Table I. EPMA results of the compositions of the IMCs at various spots

Spot code	Composition (at.%)			Phase
	Copper	Nickel	Tin	
A	52.4	2.8	44.8	(Cu,Ni) ₆ Sn ₅
B	74.8	0.0	25.2	Cu ₃ Sn
C	37.5	17.3	45.2	(Cu,Ni) ₆ Sn ₅

sputtering, and the positions 1, 2, and 3 were selected to obtain the Auger depth profiles. As shown in Fig. 5a, position 1 is located on the copper layer, position 2 is located near the interface between Cu and Cu₆Sn₅, and position 3 is located on the Cu₆Sn₅ layer. Figure 5b, c, and d show the Auger depth profiles at positions 1, 2, and 3. The results presented in Fig. 5 confirm that surface diffusion has a strong influence on the distribution of IMC in the micro-joint near the free surface, which roughens the surface. The surface diffusion phenomena had been observed in Yang's study¹⁹ and our results are very similar to his work even though the dominant diffusion species are different. However, as there is a large difference in the consumption of metals, the cross-sectional morphology of the different dominant diffusion species varies greatly.

Because of the volume shrinkage during the reaction, the morphology of the sample is often concave, as shown in Fig. 3e, f, and g. Nevertheless, Fig. 3h shows that the morphology of the sample after aging for 360 h is convex, with many voids formed near the free surface, while in Fig. 3e, f, and g, no voids are observed at the same position. Two different types of voids were formed in our study, as previously described^{6,7}. The Kirkendall void is an important part affecting the total voiding rate. Furthermore, another part contains diffusion voids, which are formed near the free surface after long-term aging. The main difference of these two types of voids is the formation mechanism. The formation of a Kirkendall void⁵ is mainly due to the different

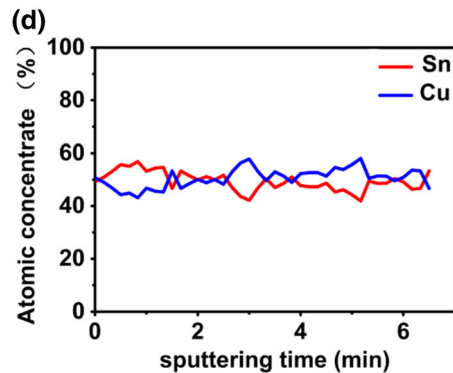
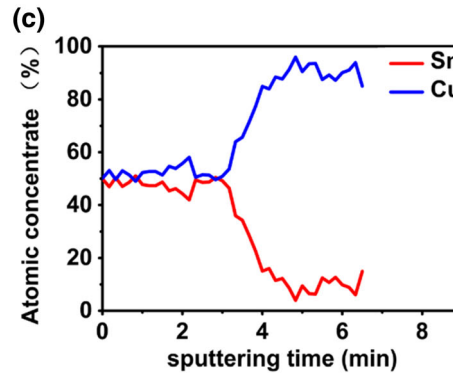
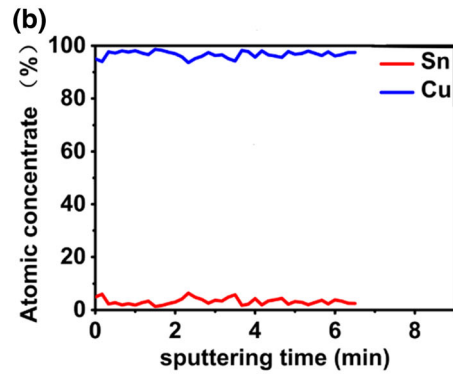
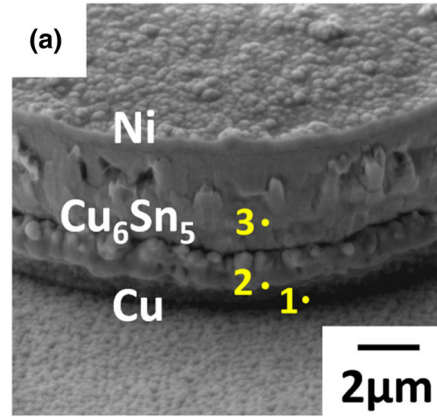


Fig. 5. Side view of the sample after aging for 24 h. (a) The sample used for Ar-ion sputtering, (b)–(d) Auger depth profiles at positions marked 1, 2, and 3 in (a).

diffusion abilities of Cu and Sn; regardless of Sn, Cu₆Sn₅ and Cu₃Sn, Cu is the dominant diffusing species; the discrepancy of Cu atoms diffusion flux

and Sn atoms diffusion flux causes the voids to form near the Cu/IMCs interface. After 24 h aging, there is almost no Sn remaining, and in order to reduce the free surface energy, the free surface morphology of the micro-joint must be changed, as the same time surface diffusion continues. This diffusion flux from IMCs to the free surface cause the defect to be formed near the free surface, and finally diffusion voids are formed. To confirm the total void rate in the micro-bump after long aging time, it is necessary to obtain cross-section images at different positions. In this study, focused ion beam (FIB) milling was used for 3D reconstruction. The sample that was aged for 720 h was selected to ensure that the aging time was long enough. Four hundred and eighty tomographic slices with an interval of 62.5 nm were sectioned by FIB. Even though the tomographic images were obtained by focused ion beam milling, the area for calculating the voiding rate must be defined because the distribution of the voids in the tomographic slices cannot represent the void distribution along the radius of the micro pillar. Figure 6a shows the top view of the schematic illustration for describing the calculation method. Three different central angles of 9.46° , 18.43° , and 26.57° were chosen for calculation. The central angles were determined by the rates of h and l in the triangles shown in Fig. 6a. The values of the rates of h and l are 3, 1.5, and 1. After determining the area for calculation, the voiding rate was calculated through the difference in the number of pixels between the voids and other areas in each image. Equation 1 was used to calculate the voiding rate.

$$\text{Voiding rate} = \frac{\text{pixels}_1 \times W_1 \times H_1}{\text{pixels}_2 \times W_2 \times H_2} \times 100\% \quad (1)$$

Pixels₁ is the number of pixels for the total voids in the chosen area, W_1 is the total width of all of the voids in the selected area, and H_1 is the total height of all of the voids in this area. Pixels₂, W_2 and H_2

are the number of pixels, the width and the height of the whole area that is chosen, respectively. Furthermore, due to the influence of the voids volume, the average voiding rate is used to represent the voiding rate at a certain position. Taking the calculation of the voiding rate on the position of $1 \mu\text{m}$ as an example, images at positions 875 nm, 937.5 nm, $1 \mu\text{m}$ (1000 nm), 1062.5 nm, and 1125 nm were selected to calculate the voiding rate of each position, and then the average of these five figures represents the voiding rate at $1 \mu\text{m}$. Finally, the relationship of the voiding rate distribution and position along the radius of the micro-bump is shown in Fig. 6b. Clearly, the shape of the curve in Fig. 6b is parabolic from the edge to the center initially, and when the distance reaches a certain range, the voiding rate becomes constant; meanwhile, from Fig. 3d and h, it is observed that after long-term aging, the morphology of the sample changes from concave to convex and, at the same time, the voids near the free surface are formed. Therefore, it can be concluded that the redistribution of the voids after long-term aging is controlled by surface diffusion when almost all IMCs become Cu_3Sn in the Cu/Sn/Ni micro-bump. Furthermore, from the result of the 3D reconstruction by FIB, it can be concluded that there is a limitation of the bump size, which has a strong effect on the reliability of the micro-bump when this limit is out of a certain range. To determine the physical limit of the micro-bump, micro-bumps with diameters of $5 \mu\text{m}$ and $10 \mu\text{m}$ were fabricated by FIB from the initial sample shown in Fig. 2. Figure 7a and b shows the side views of the $5 \mu\text{m}$ and $10 \mu\text{m}$ samples, and the samples after 720 h aging are shown in Fig. 7c and d. Using the same method, the relationship of the voiding rate and position along the radius can be obtained. Figure 7f shows a similar relationship of the curve to that in Fig. 6b, and therefore, when the diameter of the bump size decreases to $10 \mu\text{m}$, it does not reach the limitation. However, when the diameter is decreased to $5 \mu\text{m}$, the value of the

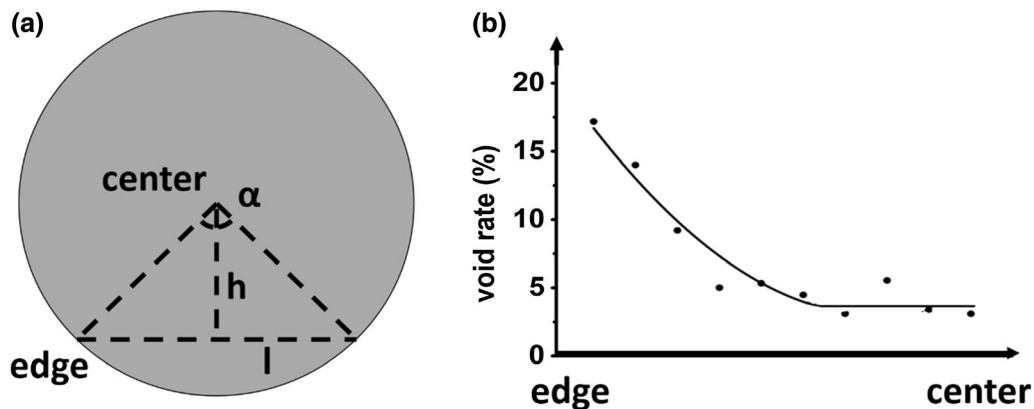


Fig. 6. (a) Top view schematic illustration to describe the calculation method. (b) Relationship of the void rate distribution along the radius direction of the sample after aging for 720 h.

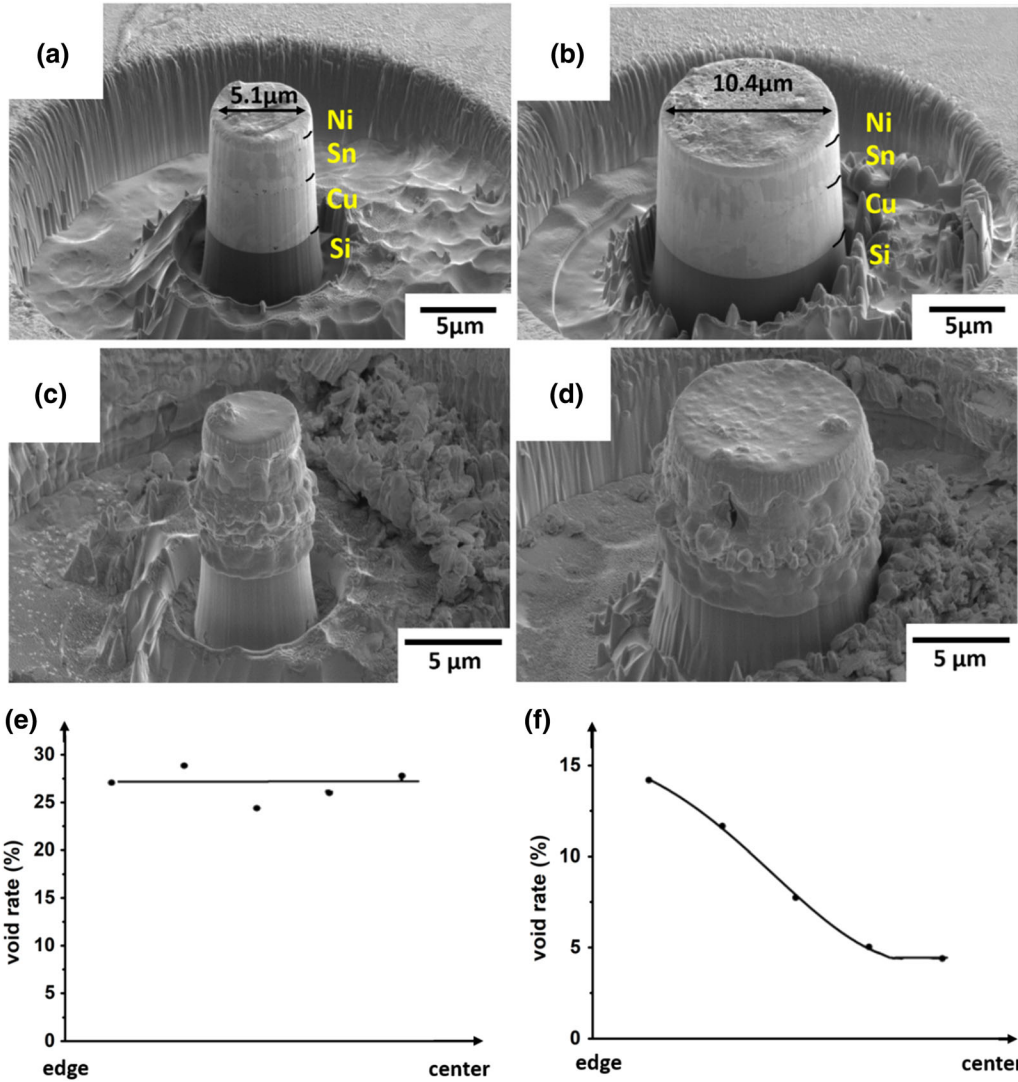


Fig. 7. (a, b) Initial samples cut by FIB with the diameters of 5 μm and 10 μm ; (c, d) side views of the same samples after 720 h aging; (e, f) void rate distribution curves.

voiding rate tends to become stable, which is mainly due to the accumulation of the voids from all directions. When the bump size reaches its limit, the voiding rate is approximately two times greater than the voiding rate of the other two bump sizes. A higher voiding rate may lead to the mechanical deterioration of the micro-bump. Taken together, these results indicate that the bump size has a strong influence on the reliability of the micro-joint, particularly when the diameter of the micro-bump is decreased to 5 μm or even to less than 5 μm .

CONCLUSION

An electroplated Cu/Sn/Ni micro-bump was fabricated for analysis. After aging for different times, both the morphology and microstructure show significant changes, particularly after long-term aging. Because of the small aspect ratio of the micro-bump, surface diffusion has a strong effect on the

morphology and roughness of the Cu/Sn and Cu/IMCs interfaces. In the Cu/Sn/Ni system, Cu is the dominant diffusion species, and the large consumption of Cu, particularly near the free surface, leads to the concave morphology in the copper layer. FIB was applied for 3D reconstruction and used for calculation of the voiding rate of the micro-joint after 720 h of aging. In this way, the relationship between the voiding rate redistribution and the position along the radius direction was obtained. It is concluded that the redistribution of voids after long-term aging is controlled by surface diffusion when almost all of the IMCs in the Cu/Sn/Ni micro-bump were transformed to Cu_3Sn . Furthermore, as observed from the relationship between the voiding rate of the 5 μm and 10 μm samples and the position along the radius, when the diameter of the micro-bump decreases to 5 μm or even less than 5 μm , the total voiding rate of the sample after long-term aging rapidly increases, and a higher voiding rate

has a strong influence on the reliability of the micro-joint and may lead to the failure of the electronic device. After long-term aging, a high Ni content $(\text{Cu,Ni})_6\text{Sn}_5$ phase was formed in the middle and near the Ni side of the micro bump. Additionally, even when the aging time reaches 1000 h, $(\text{Cu,Ni})_6\text{Sn}_5$ is still present because the Ni content of $(\text{Cu,Ni})_6\text{Sn}_5$ reaches its limit, and this high Ni content phase is stable in the solid-state reaction. The formation of the high Ni content $(\text{Cu,Ni})_6\text{Sn}_5$ is explained as follows: due to the difference in the maximum solubility limit of Ni contents, when Cu_6Sn_5 changes to Cu_3Sn , some Ni atoms must diffuse along the Cu_6Sn_5 grain boundary, continuously increasing the Ni content, and when the Ni content reaches its solubility limit, $(\text{Cu,Ni})_6\text{Sn}_5$ become a stable phase and Cu atoms from the Cu side cannot react with it; consequently, these Cu atoms must travel to the other parts to form Cu_3Sn . As a result, the high-Ni-content $(\text{Cu,Ni})_6\text{Sn}_5$ will be surrounded by Cu_3Sn . Further, with abundant Ni supplied by the Ni side, a stable $(\text{Cu,Ni})_6\text{Sn}_5$ was also formed near the electroplated Ni. However, further experiments and analyses are needed to elucidate the microstructure and further details of the high-Ni-content $(\text{Cu,Ni})_6\text{Sn}_5$.

ACKNOWLEDGMENTS

The funding support of the Ministry of Education (108L9006), Ministry of Science and Technology of Taiwan (107-2622-E-002-004-CC2 and 108-3017-F-002-002), and National Taiwan University (NTU-CC-107L892401) are acknowledged. The Advanced Research Center for Green Materials Science and Technology is supported by the Featured Areas Research Center Program within the framework of the Higher Education Sprout Project of Taiwan.

REFERENCES

1. K.N. Tu and R.D. Thompson, Kinetics of interfacial reaction in bimetallic Cu-Sn thin films. *Acta Metall.* 30, 947 (1982).
2. K.N. Tu, Interdiffusion and reaction in bimetallic Cu-Sn thin films. *Acta Metall.* 21, 347 (1973).
3. C.R. Kao, Microstructures developed in solid-liquid reactions: using Cu-Sn reaction, Ni-Bi reaction, and Cu-In reaction as examples. *Mater. Sci. Eng., A* 238, 196 (1997).
4. C.K. Chung, J.G. Duh, and C.R. Kao, Direct evidence for a Cu-enriched region at the boundary between Cu_6Sn_5 and Cu_3Sn during Cu/Sn reaction. *Scr. Mater.* 63, 258 (2010).
5. K. Zeng, R. Stierman, T.C. Chiu, D. Edwards, K. Ano, and K.N. Tu, Kirkendall void formation in eutectic SnPb solder joints on bare Cu and its effect on joint reliability. *J. Appl. Phys.* 97, 024508 (2005).
6. J. Yu and J.Y. Kim, Effects of residual S on Kirkendall void formation at Cu/Sn–3.5Ag solder joints. *Acta Mater.* 56, 5514 (2008).
7. Y.W. Wang, Y.W. Lin, and C.R. Kao, Kirkendall voids formation in the reaction between Ni-doped SnAg lead-free solders and different Cu substrates. *Microelectron. Reliab.* 49, 248 (2009).
8. L. Yin and P. Borgesen, On the root cause of Kirkendall voiding in Cu_3Sn . *J. Mater. Res.* 26, 455–466 (2011).
9. C.M. Tsai, W.C. Luo, C.W. Chang, Y.C. Shieh, and C.R. Kao, Cross-interaction of under-bump metallurgy and surface finish in flip-chip solder joints. *J. Electron. Mater.* 33, 1424–1428 (2004).
10. C.S. Liu, C.E. Ho, C.S. Peng, and C.R. Kao, Effects of joining sequence on the interfacial reactions and substrate dissolution behaviors in Ni/solder/Cu joints. *J. Electron. Mater.* 40, 1912–1920 (2011).
11. C.E. Ho, S.C. Yang, and C.R. Kao, Interfacial reaction issues for lead-free electronic solders, in *Lead-Free Electronic Solders* (Springer, Boston, 2006), pp. 155–174.
12. K. Nogita and T. Nishimura, Nickel-stabilized hexagonal $(\text{Cu, Ni})_6\text{Sn}_5$ in Sn-Cu-Ni lead-free solder alloys. *Scr. Mater.* 59, 191 (2008).
13. K. Nogita, C.M. Gourlay, S.D. McDonald, Y.Q. Wu, J. Read, and Q.F. Gu, Kinetics of the η - η' transformation in Cu_6Sn_5 . *Scr. Mater.* 65, 922 (2011).
14. D. Mu, J. Read, Y. Yang, and K. Nogita, Thermal expansion of Cu_6Sn_5 and $(\text{Cu, Ni})_6\text{Sn}_5$. *J. Mater. Res.* 26, 2660 (2011).
15. D. Mu, H. Huang, and K. Nogita, Anisotropic mechanical properties of Cu_6Sn_5 and $(\text{Cu, Ni})_6\text{Sn}_5$. *Mater. Lett.* 86, 46 (2012).
16. L. Mo, C. Guo, Z. Zhou, F. Wu, and C. Liu, Microstructural evolution of Cu–Sn–Ni compounds in full intermetallic micro-joint and in situ micro-bending test. *J. Mater. Sci.: Mater. Electron.* 29, 11920 (2018).
17. Y.S. Kaganovskii, L.N. Paritskaya, and W. Lojkowski, *Surf. Sci.* 454–456, 591 (2000).
18. H.K. Cheng, Y.J. Lin, H.C. Chang, K.C. Liu, Y.L. Wang, T.F. Liu, and C.M. Chen, *Metall. Mater. Trans. A* 46, 1834 (2015).
19. H.W. Yang, J.Y. Wu, Z.X. Zhu, and C.R. Kao, Effects of surface diffusion and reaction-induced volume shrinkage on morphological evolutions of micro joints. *Mater. Chem. Phys.* 191, 13–19 (2017).
20. H.W. Yang, H.Y. Yu, and C.R. Kao, Critical factors affecting structural transformations in 3D IC micro joints, in *Electronic Components and Technology Conference (ECTC), 2017 IEEE 67th* (IEEE, 2017), pp. 1008–1013.
21. <http://www.geocities.jp/sato5fu/L-Vreview.htm>. Accessed 22 May 2016.

Publisher's Note Springer Nature remains neutral with regard to jurisdictional claims in published maps and institutional affiliations.